J Mater Sci (2008) 43:3750–3760
DOI 10.1007/s10853-007-2212-7

First principles study of three-component $SrTiO_3/BaTiO_3/PbTiO_3$ ferroelectric superlattices

S. H. Shah · P. D. Bristowe · A. M. Kolpak · A. M. Rappe

Received: 3 August 2007 / Accepted: 8 October 2007 / Published online: 6 March 2008

Abstract The geometrical, chemical and ferroelectric properties of a new nanoscale short-period three-component $SrTiO_3/BaTiO_3/PbTiO_3$ perovskite superlattice are investigated using a first principles density functional approach. The study focuses on varying the thickness of each component in the superlattice and determining the resulting lattice distortion and total polarization. Thicknesses of up to three unit cells in a single component are considered and the in-plane lattice constants normal to the [001] stacking direction are fixed to the bulk $SrTiO_3$ values to simulate a rigid substrate. It is found that the $PbTiO_3$ layers play a key role in strain and polarization enhancement. By increasing the amount of $PbTiO_3$ in the superlattices the strain in the other components increases significantly resulting in an enhanced total polarization of the superlattice relative to bulk $BaTiO_3$. Increasing the number of $BaTiO_3$ layers also improves the overall polarization. All the $SrTiO_3$ layers in each superlattice are found to be highly polarized. Many of the calculated features are similar to those found previously by others for the $SrTiO_3/BaTiO_3/CaTiO_3$ superlattice, although in the present study significantly greater enhancement factors and polarization values are found. The predicted enhancement of the polarization is mostly attributed to lattice strain due to mismatch of the in-plane lattice constant of the three-component materials.

S. H. Shah · P. D. Bristowe (✉)
Department of Materials Science and Metallurgy, University of Cambridge, Cambridge CB2 3QZ, UK
e-mail: pdb1000@cus.cam.ac.uk

A. M. Kolpak · A. M. Rappe
Department of Chemistry, University of Pennsylvania, Philadelphia, PA 19104-6323, USA

Introduction

There is considerable research activity into the design and characterization of ferroelectric superlattices (SL) since experimental measurements and theoretical investigations have shown that they can display superior functional properties relative to single-component ferroelectric materials in either bulk or thin-film form. Ferroelectric SLs are artificially structured multilayers composed of two or more thin-film perovskite components such as $BaTiO_3$ (BT), $PbTiO_3$ (PT) and $CaTiO_3$ (CT). The components themselves need not all be ferroelectric or chemically uniform. Incipient ferroelectrics such as $SrTiO_3$ (ST), metallic oxides such as $SrRuO_3$ and solid solutions have been used with similar effects obtained. By varying the number of components, their thickness, composition and sequence in the multilayer it may be possible to achieve a significant enhancement in dielectric properties such as spontaneous polarization which will undoubtedly benefit future device applications. The polarization increase is clearly related to the lattice strain induced in the multilayer by interfacing components with different structural parameters, ferroelectric distortions and ionic charges. The optimal combination of parameters which maximizes the functional properties is not obvious and understanding this has been the focus of many of the studies.

The experimental fabrication of ferroelectric SLs with controlled composition and structure requires the use of epitaxial deposition techniques such as MBE and PLD. With these techniques it is possible to engineer the SLs while minimizing the introduction of lattice defects, dislocations and interfacial steps that may degrade the polarization effects. The structural quality of the multilayers can be assessed using various electron microscopy and diffraction techniques [1]. The simplest type of SL involves just two

components having layers of varying thickness. Recent bilayer systems investigated include $BaTiO_3/BaO$ [2], $SrTiO_3/SrO$ [2], $BaTiO_3/SrTiO_3$ [3–7], $PbTiO_3/SrTiO_3$ [8–11], $PbTiO_3/PbZrO_3$ [12], $SrZrO_3/SrTiO_3$ [13–15], $KNbO_3/KTaO_3$ [16], $PbTiO_3/BaTO_3$ [17–20], $PbTiO_3/SrRuO_3$ [21] and modulated $PbZr_{1-x}Ti_xO_3$ (PZT) [22] and $PbSc_{1-x}Nb_xO_3$ (PSN) [23]. In addition to determining strain and polarization effects, the evolution and stability of different phases has been studied [24, 25]. Computationally various atomistic approaches have been taken to calculate the structure and properties of SLs. The level of theory employed determines the size of the system that can be studied and the accuracy of the results. The investigations include density functional (DFT) calculations [2–5, 21, 26] the first of which was on the $Pb(Zr_{0.5}Ti_{0.5})O_3$ system [27, 28]. Other studies have used empirical shell-model calculations [29], effective Hamiltonian methods [23, 30] and electrostatic methods [10]. Emerging from this body of experimental and theoretical work are three key factors which influence the enhancement of SL polarization: the mismatch between the lattice parameters of the components, the difference between the dielectric constants of the components and the structure and chemistry of the interphase boundaries between the components.

Introducing a third perovskite into the superlattice is an obvious extension to the bilayer system and can have the fundamental effect of changing its symmetry. Sai et al. [31] predicted the properties of these superlattices, which have general formulae $\left(A_{1/3}A'_{1/3}A''_{1/3}\right)BO_3$ and $A\left(B_{1/3}B'_{1/3}\ B''_{1/3}\right)O_3$, by focusing on the effect of compositionally breaking the inversion symmetry. Following the theoretical predictions, experimental studies on the $SrTiO_3/BaTiO_3/CaTiO_3$ (ST/BT/CT) system were performed [32, 33]. Warusawithana et al. [33] utilized the broken inversion symmetry of the ST/BT/CT trilayer SL and obtained a very large dielectric constant (10^3 at room temperature) for the system. Lee et al. [32] also prepared ST/BT/CT superlattices on electrically conducting $SrRuO_3$ substrates using PLD. It was found that coherent superlattices with large remanent polarization can only be made if the thickness of the BT layer is less than the combined thickness of the ST and CT layers, otherwise partial strain relaxation occurs. The study verified that misfit strain alone is not enough to explain the observed/predicted enhanced polarization, but two other effects, namely interfaces and inverse symmetry breaking, must also contribute. Nakhmanson et al. [34] performed density functional calculations on ST/BT/CT superlattices and obtained increased ferroelectric polarization in the trilayer superlattice if the $BaTiO_3$ concentration is larger than 30%. Highly polarized ST and CT layers are found in such superlattices. Maximum polarization can be obtained by increasing the concentration of CT or BT layers while preserving the overall strain. Interestingly it is found that trilayer superlattices have two values of polarization depending on the direction of the ferroelectric displacement. Nakhmanson et al. [35] also used DFT calculations to construct a general model that optimizes the combination of CT, BT and ST layers and predicts structures with maximum polarization and minimum lattice mismatch.

In this article a first principles study of the properties of another short-period trilayer superlattice, $(SrTiO_3)_x/(BaTiO_3)_y/(PbTiO_3)_z$, where $x, y, z = 1, 2, 3$ is presented. The possibility of improving the ferroelectric properties of the SL is investigated by varying the layer thicknesses. Some bilayer superlattices are also studied for comparison purposes. The results are compared with other computational and experimental work where possible. Details of the computational method are given in the next section followed by the results, discussion and conclusions.

Computational method

The first principles calculations are performed using a density functional, plane-wave pseudopotential approach [36] which is implemented in the CASTEP program [37]. The method is used to optimize the geometries of bulk, bilayer and trilayer superlattices involving $SrTiO_3$, $BaTiO_3$ and $PbTiO_3$. Optimized norm-conserving pseudopotentials [38] are used for the electron-ion interactions with the following valence states treated explicitly: Ba(5s,5p,6s), Ti(3s,3p,3d,4s), O(2s,2p), Sr(4s,4p,5s) and Pb(5d,6s,6p). The potentials for Ba, Ti and O were constructed using the Opium code [39] and used the designed nonlocal approach of Ramer and Rappe [40–43]. A plane-wave kinetic energy cutoff of 700 eV is employed which is sufficient to achieve convergence to less than 0.02 eV/atom. The local density approximation (LDA) with the Perdew-Zunger parameterization [44] for the exchange-correlation functional is chosen for all the calculations. Monkhorst-Pack k-point meshes with a density of $(6 \times 6 \times 6)$ points are used for bulk and strained crystals of ST, BT and PT. For the bilayers and trilayers, following Nakhmanson et al. [34], meshes with $(6 \times 6 \times N)$ points are used where $N = 6/(x + y + z)$ for $x + y + z \leq 3$, $N = 2$ for $x + y + z = 4$ and $N = 1$ for $x + y + z > 4$. These descriptions of reciprocal space were found sufficient for convergence purposes in previous calculations [34, 45] and in the present study as well. The initial geometries are optimized by the BFGS minimizer [46]. The convergence thresholds between geometry optimization cycles for energy change, maximum force, maximum stress and maximum displacement are set as 5×10^{-6} eV/atom, 0.01 eV/Å, 0.02 GPa and 5×10^{-4} Å, respectively. The optimization terminates when all these criteria are satisfied.

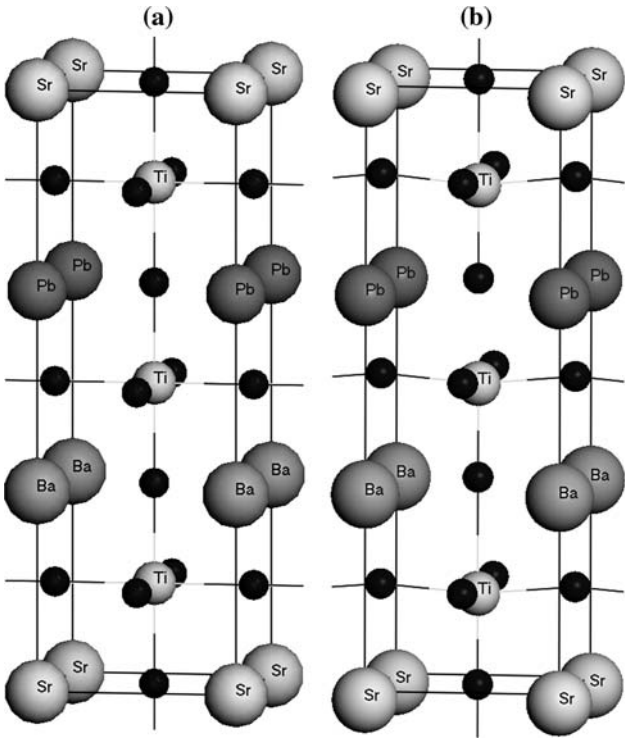

Fig. 1 The atomic structure of the $SrTiO_3/BaTiO_3/PbTiO_3$ ($ST_1BT_1PT_1$) superlattice: (**a**) unrelaxed and (**b**) relaxed. The unlabelled black circles are oxygen ions. The circles are not in proportion to the ionic radii. The vertical direction is [001]

The trilayers in the computational supercell are constructed sequentially starting at the lower end with $SrTiO_3$ (cubic), then adding $BaTiO_3$ (tetragonal) and finally $PbTiO_3$ (tetragonal) in various proportions. Figure 1 illustrates the equi-component case where $x = y = z = 1$. The supercell is oriented such that the superlattice extends along the [001] direction. For all the bulk, strained, bilayer and trilayer systems studied no particular symmetry is imposed during the calculations. This differs from many previous calculations (e.g., [34]) which impose a restricted symmetry condition that allows relaxation only along [001]. In the strained, bilayer and trilayer systems, however, the (001) in-plane lattice parameter is constrained to the optimized value of fully relaxed bulk $SrTiO_3$ so that this material then acts as a substrate.

Results and discussion

As a first step, the structures of all three constituents of the ST/BT/PT superlattice in their bulk and strained phases are optimized. The results are presented in Tables 1–3. It is seen that the optimized geometries are in good agreement with previous DFT calculations and experimental results.

Then for each system, linear response calculations are performed to obtain the Born effective charges of each species in the respective phase. The Born effective charge is a tensor quantity defined as

$$Z^*_{k,\alpha\beta} = \Omega_o \frac{\partial P_\beta}{\partial u_{k\alpha}}|_{E=0} \quad (1)$$

where P_β is the total polarization per unit cell generated in β direction, $u_{k\alpha}$ is a rigid displacement of the sublattice of atom k in the α direction and Ω_o is the unit cell volume [55]. Tables 4–6 show the diagonal elements of the calculated Born effective charges with comparisons to values obtained by other DFT calculations. Once again it is seen that the values are in good agreement with previous work. The Born effective charges are used to calculate the spontaneous polarization of the bulk, strained, bilayer and trilayer systems. These charges are sensitive to the atomic displacements, but their values do not change very much for small strains. In the present calculations the use of Born effective charges determined from bulk crystals will not change the basic results derived for the superlattices. To calculate the local polarization in a unit cell the following expression is used [34]:

$$P_\lambda = \sum_i \frac{\partial P}{\partial u^{(o)}_{\lambda i}}(u_{\lambda i} - u^{(o)}_{\lambda i}) = \frac{1}{\Omega_\lambda}\sum_i Z^*_{\lambda i}\Delta u_{\lambda i} \quad (2)$$

where Ω_λ is the volume of a unit cell λ, $Z^*_{\lambda i}$ is the Born effective charge of ion i in this cell and $\Delta u_{\lambda i}$ is the displacement of ion i in this cell. The superscript zero refers to the reference structure which is nonpolar and centrosymmetric. The same general expression can be used to calculate the total polarization of a superlattice containing many unit cells by summing over all atoms in the SL structure. Previous studies [34] have shown that the total polarization obtained this way agrees well with equivalent values obtained using the Berry phase approach [57].

Geometrical structure and lattice distortions

One convenient measure of the lattice distortion or strain in a relaxed superlattice is the axial ratio *c/a* in the component layers and how it changes relative to a reference value that is determined from a bulk crystal or another superlattice. Another way of describing the lattice distortions is to determine the displacements of the ions in the relaxed superlattice with respect to an equivalent centrosymmetric structure, the so-called off-centre displacements. To allow for comparison with previous computational studies both approaches are taken here.

Table 1 The optimized structural parameters of $SrTiO_3$ obtained in the present study compared to experimental work and two other computational investigations

Parameters	Experimental [47]	Present study	Reference [48]	Reference [2]
a (Å)	3.905	3.856	3.85	3.874
b (Å)	3.905	3.856	3.85	3.874
c (Å)	3.905	3.856	3.85	3.874
c/a	1	1	1	1
V (Å^3)	59.547	57.339	57.067	58.141
$Sr_{(z\text{-component})}$	0	0	0	0
$Ti_{(z\text{-component})}$	0.5	0.5	0.5	0.5
$O_1 = O_{2(z\text{-component})}$	0.5	0.5	0.5	0.5
$O_{3(z\text{-component})}$	0	0	0	0

Table 2 The optimized structural parameters of $BaTiO_3$ obtained in the present study compared to experimental work and two other computational investigations

Parameters	Experimental [49]	Present study	Reference [50][a]	Reference [51][a]
a (Å)	3.995	3.939	3.994	3.994
b (Å)	3.995	3.939	3.994	3.994
c (Å)	4.034	3.993	4.036	4.036
c/a	1.010	1.014	0.990	0.990
V (Å^3)	64.359	61.941	64.382	64.382
$Ba_{(z\ \text{component})}$	0	0	0	0
$Ti_{(z\ \text{component})}$	0.514	0.515	0.514	0.522
$O_1 = O_{2(z\ \text{component})}$	0.488	0.486	0.481	0.490
$O_{3(z\ \text{component})}$	−0.025	−0.022	−0.031	−0.023

[a] Calculations performed at fixed experimental volume

Table 3 The optimized structural parameters of $PbTiO_3$ obtained in the present study compared to experimental work and two other computational investigations

Parameters	Experimental [52]	Present study	Reference [53][a]	Reference [54][b]
a (Å)	3.904	3.793	3.834	3.904
b (Å)	3.904	3.793	3.834	3.904
c (Å)	4.152	4.231	4.302	4.151
c/a	1.064	1.116	1.122	1.063
V (Å^3)	63.282	60.882	63.238	63.266
$Pb_{(z\ \text{component})}$	0	−0.0314	0	0
$Ti_{(z\ \text{component})}$	0.540	0.527	0.542	0.549
$O_1 = O_{2(z\ \text{component})}$	0.612	0.633	0.634	0.630
$O_{3(z\ \text{component})}$	0.112	0.115	0.134	0.125

[a] Optimized c/a at constant volume, LDA, all-electron basis set

[b] Constant volume and c/a, LDA, ultrasoft pseudopotentials with plane-wave basis

To begin with, it is of interest to determine how distorted the bulk unit cells of BT and PT become when their in-plane a lattice parameters are constrained to the corresponding bulk value of ST. This constraint is performed to simulate the mechanical effect of the rigid ST substrate. The results show that the BT c/a increases by 5.05% while the corresponding ratio for PT decreases by 5.24%. These values are comparable to results obtained from experimental [49, 52] and other theoretical investigations [50, 51, 53, 54].

Consider now the three symmetric bilayer superlattices ST_xBT_x ($x = 1, 2$) and ST_1PT_1. The c/a ratios for the complete superlattices and for the individual components (averaged when $x > 1$) are given in Table 7. For the ST_xBT_x superlattices, the average c/a in the ST layers increases while that of the BT layers decreases compared to that of the calculated bulk-constrained ST and BT crystals, respectively. For the ST_1PT_1 superlattice, the average c/a increases by a small amount in the ST layer while in the PT layer it decreases when compared to the calculated bulk-constrained ST and PT crystals.

The structures of the bilayer SLs can be compared to the trilayer SLs to determine the effect of inserting another component. For example, it is found that adding a PT layer on top of the ST_1BT_1 superlattice to create a trilayer $ST_1BT_1PT_1$ superlattice increases the c/a ratio in the ST layer by about 2.60% and decreases the corresponding ratio in the BT layer by 1.5%. If the thickness of the PT layer is

Table 4 The Born effective charge tensor for tetragonal $SrTiO_3$ calculated in the present study and compared to two other computational investigations

Elements	Present study	Reference [55]	Reference [56]
Z^*_{Sr}	2.56	2.56	2.55
Z^*_{Ti}	7.40	7.26	7.56
$Z^*_{O_1}$	−2.08	−2.15	−2.12
$Z^*_{O_2}$	−2.08	−2.15	−2.12
$Z^*_{O_3}$	−5.81	−5.73	−5.92

Table 5 The Born effective charge tensor for tetragonal $BaTiO_3$ calculated in the present study and compared to another computational investigation

Elements	Present study	Reference [55]
Z^*_{Ba}	[2.74 2.74 2.80]	[2.72 2.72 2.83]
Z^*_{Ti}	[7.19 7.19 6.17]	[6.94 6.94 5.81]
$Z^*_{O_1}$	[−5.72 −2.15 −2.01]	[−5.53 −2.14 −1.95]
$Z^*_{O_2}$	[−2.15 −5.72 −2.01]	[−2.14 −5.53 −1.95]
$Z^*_{O_3}$	[−2.06 −2.06 −4.95]	[−1.99 −1.99 −4.73]

The diagonal elements Z^*_{xx}, Z^*_{yy} and Z^*_{zz} of the tensor are presented here as [Z^*_{xx} Z^*_{yy} Z^*_{zz}]

Table 6 The Born effective charge tensor for tetragonal $PbTiO_3$ calculated in the present study and compared to another computational investigation

Elements	Present Study	Reference [53]
Z^*_{Pb}	[3.70 3.70 3.08]	[3.74 3.74 3.52]
Z^*_{Ti}	[5.74 5.74 5.21]	[6.20 6.20 5.18]
$Z^*_{O_1}$	[−4.80 −2.69 −2.01]	[−5.18 −2.16 −2.16]
$Z^*_{O_2}$	[−2.69 −4.80 −2.01]	[−2.61 −5.18 −2.16]
$Z^*_{O_3}$	[−1.94 −1.94 −4.26]	[−2.15 −2.15 −4.38]

The diagonal elements Z^*_{xx}, Z^*_{yy} and Z^*_{zz} of the tensor are presented here as [Z^*_{xx} Z^*_{yy} Z^*_{zz}]

increased in $ST_1BT_1PT_z$ superlattices it further increases the *c/a* ratio in the ST layers and also induces an increase in *c/a* ratio in the BT layers. Similarly, comparing the ST_1PT_1 superlattice with the $ST_1BT_1PT_1$ superlattice it is found that introducing a single BT layer in between the ST and PT layers also increases the *c/a* ratio in the ST layer, this time by 4.23%, while it slightly decreases *c/a* in the PT layer by 0.42%. On the other hand, if the number of BT layers is increased to 2 or 3, the *c/a* ratio in the ST and PT layers increases compared to $ST_1BT_1PT_1$. However, $ST_1BT_2PT_1$ is an exception since the *c/a* ratio in the ST layer decreases slightly in this case.

The lattice distortion of different trilayer SLs can be compared when the relative composition of the components is changed. In trilayer $ST_xBT_1PT_1$ superlattices, the addition of ST layers is seen to decrease the average *c/a*

Table 7 Calculated *c/a* ratios for complete superlattices $ST_xBT_yPT_z$ and for individual components ST, BT and PT averaged over the number of layers in the component

Superlattice	*c/a*	$\langle c/a\rangle_{ST}$	$\langle c/a\rangle_{BT}$	$\langle c/a\rangle_{PT}$
ST_1BT_1	2.056 (2.07*E*, 2.042*T*)	1.023	1.033	
ST_2BT_2	4.121 (4.088*T*)	1.014	1.046	
ST_1PT_1	2.037	1.008		1.030
$ST_1BT_1PT_1$	3.093	1.050	1.018	1.025
$ST_2BT_1PT_1$	4.086	1.027	1.015	1.018
$ST_3BT_1PT_1$	5.093	1.020	1.016	1.018
$ST_1BT_2PT_1$	4.156	1.050	1.041	1.026
$ST_1BT_3PT_1$	5.227	1.053	1.049	1.026
$ST_1BT_1PT_2$	4.138	1.063	1.019	1.028
$ST_1BT_1PT_3$	5.194	1.076	1.025	1.031
$ST_1BT_2PT_2$	5.203	1.060	1.045	1.026

Values in parentheses are listed from ref. [34], *E* = experimental. *T* = theoretical

ratio of the ST layers. However, the average *c/a* ratio of the BT layers in $ST_1BT_yPT_1$ superlattices is found to increase as the thickness of the BT layers is increased. Similarly, in $ST_1BT_1PT_z$ superlattices an increase in the number of PT layers increases the average *c/a* ratio in the PT layers. Furthermore an increase in the number of BT and PT layers in $ST_1BT_yPT_z$ superlattices also causes an increase in the average *c/a* ratio of the BT and PT layers when compared to $ST_1BT_1PT_1$.

By increasing the thickness of the ST layer in $ST_xBT_1PT_1$ superlattices a slight increase in the *c/a* ratio of the BT layer is observed whereas the ratio in the PT layer remains constant. On the other hand, an increase in the BT layer thickness in $ST_1BT_yPT_1$ superlattices is seen to increase the *c/a* ratio in the ST layer and slightly in the PT layer as well. Similarly, an increase of the PT layer thickness in $ST_1BT_1PT_z$ superlattices causes a large increase in the *c/a* ratio in the ST layer with increases in the BT layer also. These results show that the lattice distortion in $ST_xBT_yPT_z$ superlattices can be manipulated by changing the layer thicknesses and the goal is to do so in such as way as to enhance its functional properties.

Figure 2a–c illustrates the off-centre displacements of the *A* cations (Sr, Ba and Pb) for the $ST_xBT_1PT_1$, $ST_1BT_1PT_z$ and $ST_1BT_yPT_1$ superlattices with respect to the amount of ST, PT and BT present. When there is more than one unit cell of a component in the SL then the displacement plotted is an average value for the cation concerned. It is seen that as the thickness of the PT layer increases in the $ST_1BT_1PT_z$ system, the average ferroelectric displacement of the Pb atoms from their centrosymmetric positions also increases quite significantly. It also increases the off-centre displacement of the Sr atom whereas it does not appreciably move the Ba atom

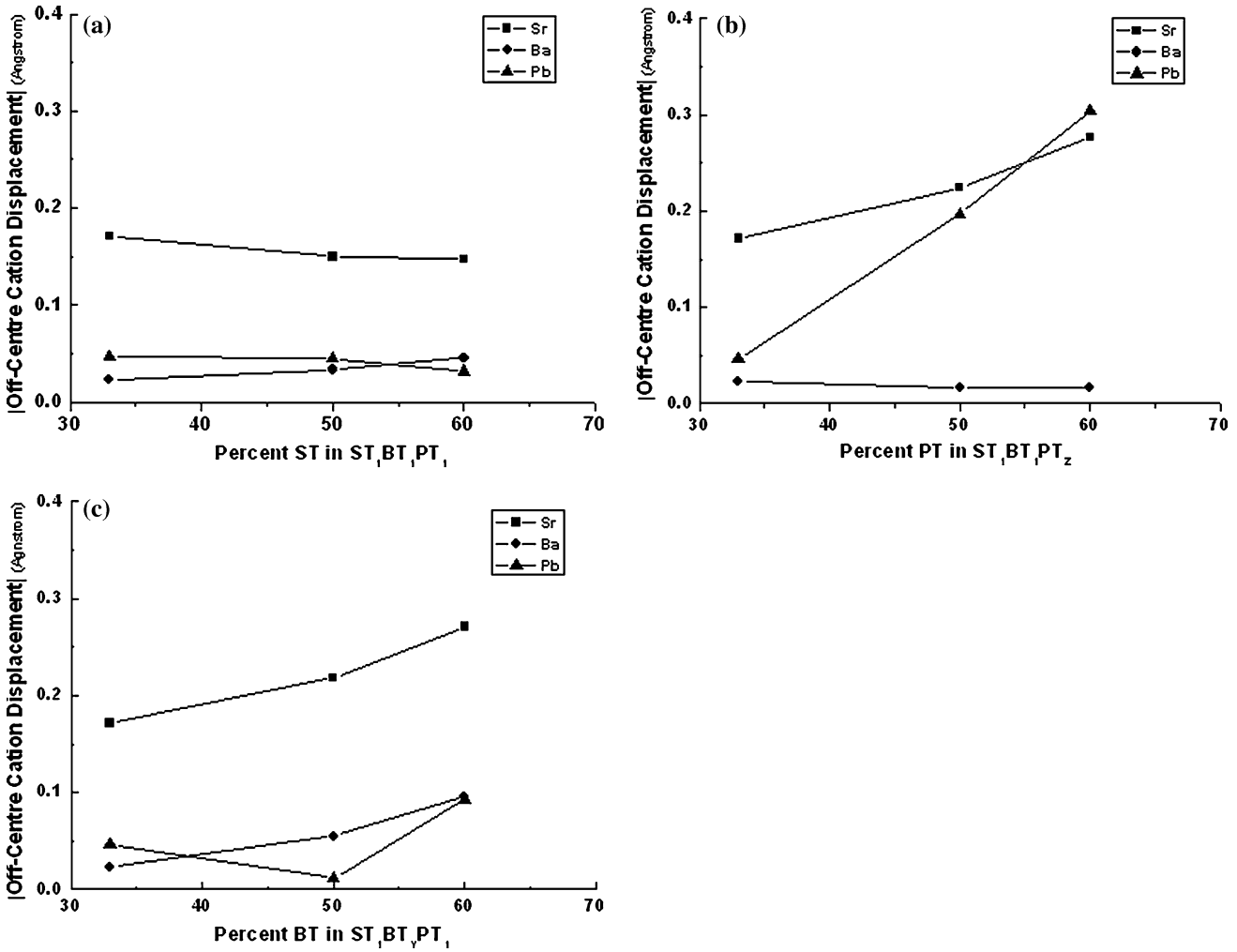

Fig. 2 The off-centre displacements of the *A* cations (Sr, Ba and Pb) in the superlattice with respect to the amount of majority component (**a**) % ST in $ST_xBT_1PT_1$; (**b**) %PT in $ST_1BT_1PT_z$; and (**c**) %BT in $ST_1BT_yPT_1$

from its initial position. Similarly as the BT layer thickness is increased in the $ST_1BT_yPT_1$ system, the Pb and Ba atoms gradually increase their off-centre displacement. The Sr atom also moves away from its centrosymmetric position in a similar fashion. On the other hand, increasing the ST layer thickness does not systematically increase the displacements of the Sr, Ba or Pb cations in the $ST_xBT_1PT_1$ system. Large ferroelectric displacements of cations in thick PT and BT superlattices make their local and, consequently total, polarization appreciably large. It is also interesting to note the displacement pattern of different ions. In bulk and constrained BT, the ferroelectric displacements of the *A* (Ba), *B* (Ti) and O ions are similar, that is cations and anions move in opposite directions. Similarly in bulk and constrained PT, Pb ions move in the opposite direction to Ti and O ions. In all the superlattices all the cations move in the same direction as the thickness of a particular layer is increased.

Local and total polarization

The displacement of atoms in ferroelectric perovskites and the distortion of their unit cells induce polarization. Table 8 lists the calculated total polarization in the various bulk crystals and ST/BT/PT superlattices studied in this work. Equation 2 is used to compute the polarization using the Born effective charges determined from linear response calculations. Also listed is a commonly used measure of the change in polarization, the polarization enhancement factor [3, 34] which is calculated relative to the polarization of bulk tetragonal BT. Considering first the bulk structures, it is seen that when constrained to the ST in-plane lattice parameter, bulk BT has a significantly greater polarization compared to its unstrained state (59.6%). However, the polarization in constrained PT decreases by 15.1% compared to its unstrained state. This shows that the ST constraint favours polarization enhancement in BT but

Table 8 The total polarization and enhancement factor for bulk and constrained crystals of ST, BT and PT and also ST_x BT_y PT_z superlattices determined using Eq. 2

System	Total polarization |P| (C/m^2)	$\|P\|/\|P\|_{Bulk\ BT}$
ST	0	0
BT	0.265 (0.27*E* [58], 0.243*T* [34], 0.30 *T* [59])	1
PT	1.094 (0.75*E* [59], 0.88*T* [53])	4.128
ST(constrained)	0	0
BT (constrained)	0.423 (0.368*T* [34])	1.596
PT(constrained)	0.928 (0.73*T* [10])	3.502
ST_1 BT_1	0.305 (0.059*E* [34], 0.231*T* [34])	1.151 (0.54*E* [34], 0.95T [34])
ST_2 BT_2	0.335 (0.306*T* [34])	1.264 (1.26*T* [34])
ST_1 PT_1	0.527	1.989
ST_1 BT_1 PT_1	0.398	1.502
ST_2 BT_1 PT_1	0.357	1.347
ST_3 BT_1 PT_1	0.369	1.392
ST_1 BT_2 PT_1	0.418	1.577
ST_1 BT_3 PT_1	0.421	1.589
ST_1 BT_1 PT_2	0.475	1.792
ST_1 BT_1 PT_3	0.632	2.385
ST_1 BT_2 PT_2	0.503	1.898

Values in parentheses are listed from other studies, *E* [ref] = experimental. *T* [ref] = theoretical

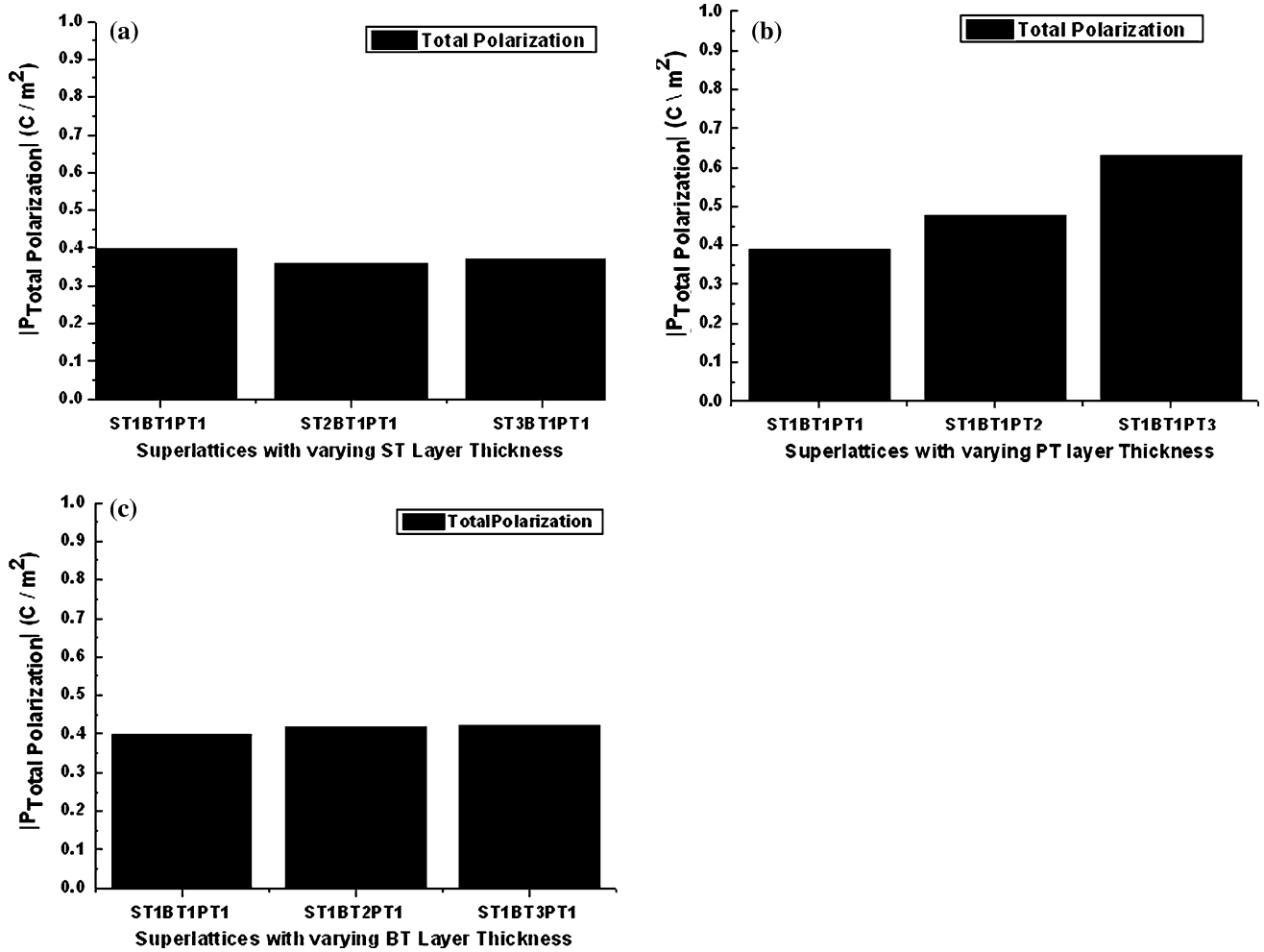

Fig. 3 The calculated total polarization of the superlattice as a function of the number of component layers (**a**) $ST_xBT_1PT_1$ $x = 1,2,3$; (**b**) $ST_1BT_1PT_z$ $z = 1,2,3$; and (**c**) $ST_1BT_yPT_1$ $y = 1,2,3$

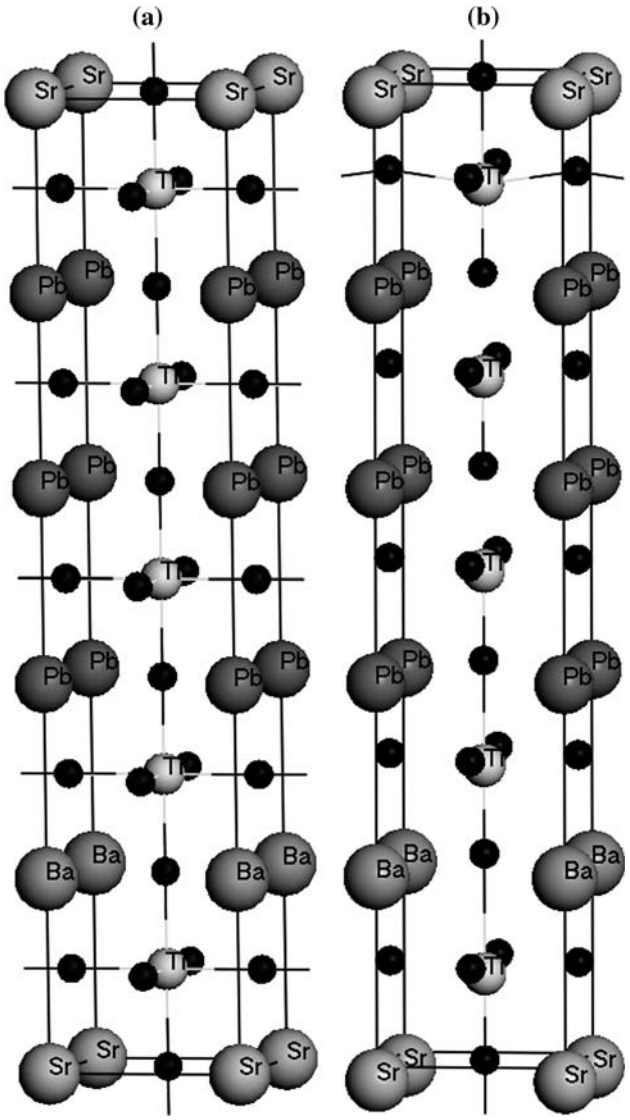

Fig. 4 The atomic structure of the $ST_1BT_1PT_3$ superlattice: (**a**) unrelaxed and (**b**) relaxed. The unlabelled black circles are oxygen ions. The circles are not in proportion to the ionic radii. The vertical direction is [001]

not PT. The computed values of the bulk polarization, both strained and unstrained, are encouragingly close to experimental data and previous calculations.

The total polarization in the ST_xBT_x bilayer superlattices is enhanced compared to bulk BT and increases as x increases. On the other hand, in the ST_1PT_1 superlattice the total polarization reduces when compared with that of bulk PT. Again the computed values are similar to previous theoretical work but larger than one experimental measurement for ST_1BT_1.

For the trilayer $ST_xBT_yPT_z$ superlattices, the total polarization is always seen to increase relative to bulk BT irrespective of the layer thicknesses. This is evident from

Fig. 5 The calculated local polarization and *c/a* ratio in individual layers across the superlattice (**a**) $ST_1BT_1PT_1$; (**b**) $ST_2BT_1PT_1$; (**c**) $ST_3BT_1PT_1$; (**d**) $ST_1BT_2PT_1$; (**e**) $ST_1BT_3PT_1$; (**f**) $ST_1BT_1PT_2$; (**g**) $ST_1BT_1PT_3$; and (**h**) $ST_1BT_2PT_2$ ▶

the enhancement factor. The increase in polarization is small in $ST_xBT_1PT_1$ superlattices and even decreases slightly as x increases (see Fig. 3a). However, for $ST_1BT_1PT_z$ superlattices the enhancement is strong and increases with increasing PT layer thickness as shown in Fig. 3b. The addition of PT layers in the superlattice clearly induces ferroelectric displacements in the ST and BT layers causing a large overall polarization enhancement compared to bulk BT. The structure of the $ST_1BT_1PT_3$ superlattice which has the largest enhancement factor is shown in Fig. 4. By increasing the number of BT layers in $ST_1BT_yPT_1$ superlattices the total polarization also increases but does so at a much slower rate than $ST_1BT_1PT_z$ superlattices (see Fig. 3c).

In all the superlattices the ST layers are highly polarized. With the application of periodic boundary conditions the PT layers introduce large ferroelectric displacements in the ST layers making them highly polar. In addition the local polarization in each component of the trilayer superlattices is found to be almost uniform across each superlattice as shown in Fig. 5a–h. This is similar to that found previously for the ST/BT/CT superlattice system [34] and has been attributed to the minimization of electrostatic energy across the interfaces [3, 15, 34]. The lattice distortion, as measured through the local *c/a* ratio in each component of each superlattice, is also found to vary uniformly across the superlattices, which is consistent with the uniformity in local polarization.

Conclusions

To summarize the present study, a series of first principles calculations have been performed on a new nanoscale trilayer $ST_xBT_yPT_z$ superlattice to investigate the effect of different stacking thicknesses and periods on its structure and total polarization. It is found that the PT layers play a key role in strain and polarization enhancement. By increasing the amount of PT in $ST_1BT_yPT_z$ superlattices the strain in the other layers i.e., ST and BT, increases significantly resulting in an enhanced total polarization of the superlattice relative to bulk BT. Similarly increasing the number of BT layers also improves the overall polarization of the trilayer superlattices. An increment in the number of ST layers, although increasing the total polarization, is not as significant an effect as increasing the

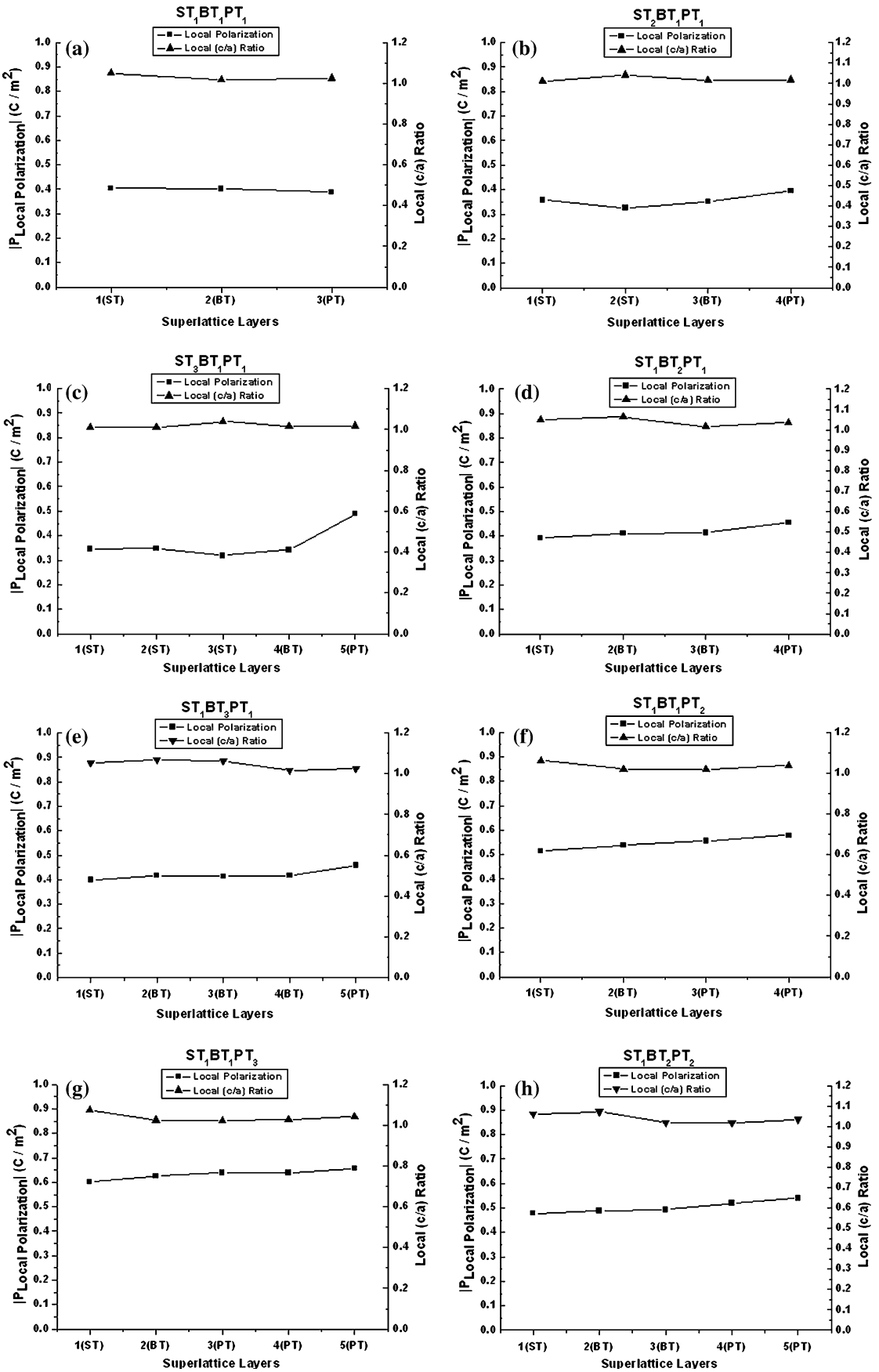
ST1BT1PT1
(a)
Local Polarization
Local (c/a) Ratio
|PLocal Polarization| (C / m2)
Local (c/a) Ratio
1(ST) 2(BT) 3(PT)
Superlattice Layers
ST2BT1PT1
(b)
1(ST) 2(ST) 3(BT) 4(PT)
ST3BT1PT1
(c)
1(ST) 2(ST) 3(ST) 4(BT) 5(PT)
ST1BT2PT1
(d)
1(ST) 2(BT) 3(BT) 4(PT)
ST1BT3PT1
(e)
1(ST) 2(BT) 3(BT) 4(BT) 5(PT)
ST1BT1PT2
(f)
1(ST) 2(BT) 3(PT) 4(PT)
ST1BT1PT3
(g)
1(ST) 2(BT) 3(PT) 4(PT) 5(PT)
ST1BT2PT2
(h)
1(ST) 2(BT) 3(BT) 4(PT) 5(PT)

amount of BT and particularly PT in the trilayer superlattices. All the ST layers in each superlattice are found to be highly polarized. In addition to that the results show approximately uniform local polarization and distortion in all layers of each superlattice studied. Many of these calculated features are similar to those found previously for the $ST_xBT_yCT_z$ superlattice [34], although for $ST_xBT_yPT_z$ we find significantly greater enhancement factors and absolute magnitudes of the local and total polarization. This predicted enhancement of the polarization is mostly attributed to lattice strain due to mismatch of the in-plane lattice constant of the three constituent perovskite materials. Finally, we note that the enhancement factor has been calculated with respect to bulk BT which is usually chosen as the standard reference material. A more stringent comparison would be to use bulk PT since it has a larger spontaneous polarization. The results show that although the $ST_xBT_yPT_z$ superlattices studied so far do not exhibit enhancement with respect to bulk PT there is a clear trend towards increasing polarization as the number of PT and BT layers are increased and therefore the system merits further investigation, both computational and experimental, to determine the effect of longer periods and different compositional sequences.

Acknowledgements Support for this work was provided by the Higher Education Commission of Pakistan, the US Office of Naval Research under grant N00014-00-1-0372 and by the US Department of Energy, Office of Basic Energy Sciences under grant DE-FG02-07ER15920. The calculations were performed using the high-performance computing facility at the University of Cambridge.

References

1. Jayadevan KP, Tseng TY (2002) J Mater Sci Mater Electronics 13:439
2. Junquera J, Zimmer M, Ordejon P, Ghosez P (2003) Phys Rev B 67:155327
3. Neaton JB, Rabe KM (2003) Appl Phys Lett 82:1586
4. Johnston K, Huang XY, Neaton JB, Rabe KM (2005) Phys Rev B 71:100103
5. Lee J, Kim L, Kim J, Jung D (2006) J Appl Phys 100:051613
6. Tian W, Jiang JC, Pan XQ (2006) Appl Phys Lett 89:092905
7. Shimuta T, Nakagawara O, Makino T, Arai S (2002) J Appl Phys 91:2290
8. Jiang JC, Pan XQ, Tan W (1999) Appl Phys Lett 74:2851
9. Lichtensteiger C, Triscone JM, Junquera J, Ghosez P (2005) Phys Rev Lett 94:047603
10. Dawber M, Lichtensteiger C, Cantoni M, Veithen M, Ghosez P, Johnston K, Rabe KM, Triscone JM (2005) Phys Rev Lett 95:177601
11. Dawber M, Lichtensteiger C, Paruch P, Triscone JM (2006) IEEE Trans Ultrason Ferr Freq Control 53:2261
12. Bungaro C, Rabe KM (2004) Phys Rev B 69:184101
13. Yang K, Wang CL, Li JC, Zhao ML, Wang XY (2006) Solid State Comm 139:144
14. Harigai T, Nam SM, Kakemoto H, Wada S, Saito K, Tsurumi T (2006) Thin Solid Films 509:13
15. Yang K, Wang C, Li J, Zhang C, Zhang R, Zhang Y, Wu Q, Lv Y, Yin N (2007) Phys Rev B 75:224117
16. Specht ED, Christen HM, Norton DP, Boatner LA (1998) Phys Rev Lett 80:4317
17. Le Marrec F, Farhi R, El Marssi M, Dellis JL, Karkut MG, Ariosa D (2000) Phys Rev B 61:R6447
18. Le Marrec F, Farhi F, Dkhil B, Chevreul J, Karkut MG (2001) J Eur Ceram Soc 21:1615
19. Le Marrec F, Farhi R, El Marssi M, Dellis JL, Ariosa D, Karkut MG (2001) Ferroelectrics 254:1
20. Le Marrec F, Farhi R, Ariosa D, El Marssi M, Dellis JL, Karkut MG (2000) Ferroelectrics 241:1769
21. Sai N, Kolpak AM, Rappe AM (2005) Phys Rev B72:020101(R)
22. Huang N, Liu Z, Wu Z, Wu J, Duan W, Gu BL, Zhang XW (2003) Phys Rev Lett 91:067602
23. George AM, Iniguez J, Bellaiche L (2001) Nature 413:54
24. Dieguez O, Rabe KM, Vanderbilt D (2005) Phys Rev B 72:144101
25. Rabe KM (2005) Curr Opin Solid State Mater Sci 9:122
26. Ghosez P, Junquera J (2006) Handbook of theoretical and computational technology, Chap. 134. American Scientific Publisher, Stevenson Ranch, CA
27. Ramer NJ, Lewis SP, Mele EJ, Rappe AM (1998) In: Cohen RE (ed) Workshop on fundamental physics of ferroelectrics. AIP, Woodbury, p 156
28. Ramer NJ, Mele EJ, Rappe AM (1998) Ferroelectrics 206:31
29. Sepliarsky M, Phillpot SR, Wolf D, Stachiotti MG, Migoni RL (2001) Phys Rev B 64:R060101
30. Iniguez J, Bellaiche L (2001) Phys Rev Lett 87:095503
31. Sai N, Meyer B, Vanderbilt D (2000) Phys Rev Lett 84:5636
32. Lee HN, Christen HM, Chisholm MF, Rouleau CM, Lowndes DH (2005) Nature 433:395
33. Warusawithana MP, Colla EV, Eckstein JN, Weissman MB (2003) Phys Rev Lett 90:036802
34. Nakhmanson SM, Rabe KM, Vanderbilt D (2005) Appl Phys Lett 87:102906
35. Nakhmanson SM, Rabe KM, Vanderbilt D (2006) Phys Rev B 73:060101
36. Payne MC, Teter MP, Allan DC, Arias TA, Joannopoulos JD (1992) Rev Mod Phys 64:1045
37. Clark SJ, Segall MD, Pickard CJ, Hasnip PJ, Probert MJ, Refson K, Payne MC (2005) Z Kristallogr 220:567
38. Rappe AM, Rabe KM, Kaxiras E, Joannopoulos JD (1990) Phys Rev B41:1227
39. http://www.opium.sourceforge.net
40. Ramer NJ, Rappe AM (1999) Phys Rev B59:12471
41. Grinberg I, Ramer NJ, Rappe AM (2000) Phys Rev B62:2311
42. Grinberg I, Ramer NJ, Rappe AM (2001) Phys Rev B63:201102(R)
43. Grinberg I, Ramer NJ, Rappe AM (2001) In: Krakauer H (ed) Workshop on fundamental physics of ferroelectrics. AIP, Melville, p 211
44. Perdew JP, Zunger A (1981) Phys Rev B 23:5048
45. King-Smith RD, Vanderbilt D (1994) Phys Rev B 49:5828
46. Fischer TH, Almlof J (1992) J Phys Chem 96:9768
47. Nakagawara O, Kobayashi M, Yoshino Y, Katayama Y, Tabata H, Kawai T (1995) J Appl Phys 78:7226
48. Johnston K, Castell MR, Paxton AT, Finnis MW (2004) Phys Rev B 70:085415
49. Evans HT (1961) Acta Cryst 14:1019
50. Ghosez P, Gonze X, Michenaud JP (1999) Ferroelectrics 220:1
51. Kwei GH, Lawson AC, Billinge SJL, Cheong SW (1993) J Phys Chem 97:2368
52. Glazer AM, Mabud SA (1978) Acta Cryst B34:1065
53. Saghi-Szabo G, Cohen RE, Krakauer H (1998) Phys Rev Lett 80:4321

54. Garcia A, Vanderbilt D (1996) Phys Rev B 54:3817
55. Ghosez P, Michenaud JP, Gonze X (1998) Phys Rev B 58:6224
56. Lasota C, Wang CZ, Yu R, Krakauer H (1997) Ferroelectrics 194:109
57. King-Smith RD, Vanderbilt D (1993) Phys Rev B 47:1651
58. Wieder HH (1955) Phys Rev 99:1161
59. Zhong W, King-Smith RD, Vanderbilt D (1994) Phys Rev Lett 72:3618